J. Non-Newtonian Fluid Mech. 165 (2010) 1536–1542

Contents lists available at ScienceDirect

Journal of Non-Newtonian Fluid Mechanics

journal homepage: www.elsevier.com/locate/jnnfm

Pressure-driven and electroosmotic non-Newtonian flows through microporous media via lattice Boltzmann method

G.H. Tang*, P.X. Ye, W.Q. Tao

State Key Lab of Multiphase Flow, School of Energy and Power Engineering, Xi'an Jiaotong University, 28 Xianning West Road, Xi'an 710049, China

ARTICLE INFO

Article history:
Received 15 June 2010
Received in revised form 10 August 2010
Accepted 13 August 2010

Keywords:
Lattice Boltzmann method
Porous media
Non-Newtonian
Electroosmotic flow

ABSTRACT

The lattice Boltzmann method is developed to simulate the pressure-driven flow and electroosmotic flow of non-Newtonian fluids in porous media based on the representative elementary volume scale. The flow through porous media was simulated by including the porosity into the equilibrium distribution function and adding a non-Newtonian force term to the evolution equation. The non-Newtonian behavior is considered based on the Herschel–Bulkley model. The velocity results for pressure-driven non-Newtonian flow agree well with the analytical solutions. For the electroosmotic flow, the influences of porosity, solid particle diameter, power law exponent, yield stress and electric parameters are investigated. The results demonstrate that the present lattice Boltzmann model is capable of modeling non-Newtonian flow through porous media.

© 2010 Elsevier B.V. All rights reserved.

1. Introduction

Transport phenomena through porous media have numerous applications in fluid mechanics, heat transfer, condensed matter, biology and environmental engineering and sciences [1] and have been the hot research subject of wide interdisciplinary concerns. In recent years, electrokinetic phenomena in microporous materials have also attracted much attention in various fields such as capillary electrochromatography and high-performance micropumps due to the large surface of porous materials, the less dispersion to an analyte and the generated high pressure of the electroosmotic porous flow, which motivates research toward a better understanding of microscale fluidic transport phenomena to optimize the device design and operation [2].

The recently developed lattice Boltzmann method (LBM), due to its inherent vantages like simple implementation, high parallelizability and great convenience to handle complex geometry and boundary conditions, has been successfully employed to study complex transport phenomena and modeling complex physics [3–6] which are usually hardly accessible to the macroscopic approaches. Generally, there exist two approaches to simulate flow in porous media by using the LBM. In the first pore-scale approach, the flow in the micropores is directly modeled by the standard LBM [7–10]. The main advantage of this approach is that detailed flow information can be obtained. However, the size of computation domain cannot be too large due to limited computer resources since each pore of the medium should contain several lattice nodes. In the second macroscale approach, modeling is made for the fluid at a representative elementary volume scale (REV) by ignoring the detailed geometry structure. This is accomplished by including an additional term to the standard lattice Boltzmann equation to account for the presence of a porous medium [11–13]. In this approach, the statistical properties of the porous structure are directly included in models. Although detailed information of fluid flow at the pore-scale is neglected, if this approach can be used in large-sized computation domain and with appropriate models, the approach can produce reasonable results. In addition, in some practical applications, such approach is the only applicable one by the numerical method based on the continuum assumption [12], at least under the present situation of computer technology. Furthermore, the LBM solution in complex porous media can obtain more useful transport information without increasing much computation efforts than directly solving a Darcy-type equation as are contained in lots of commercial flow field simulation codes.

Recent rapid development in micro-fabrication technology has enabled a variety of miniaturized fluidic systems consisting of micro ducts, valves, and pumps. The flow behavior of non-Newtonian fluid in microporous media is of high interest in practical applications such as sample collection, dispensing, reaction, detection, mixing, and separation of various biological and chemical species in capillary electrochromatography [14] and high-performance micropumps [15–17]. The fluid rheological behavior combined with the microscale effects usually plays a more important and complicated role. Fundamental understanding of the non-Newtonian role in liquid transport through microporous media is significant to correctly predict and control the character-

* Corresponding author.
E-mail address: ghtang@mail.xjtu.edu.cn (G.H. Tang).

0377-0257/$ – see front matter © 2010 Elsevier B.V. All rights reserved.
doi:10.1016/j.jnnfm.2010.08.002

istics and performance of such microfluidic devices. However, to the authors' best knowledge, the existing LBM approaches for non-Newtonian flow in porous media are all based on the pore-scale study [18–21].

The objective of this work is to develop a lattice Boltzmann model for non-Newtonian porous flow based on the REV scale. In Section 2, the numerical models for pressure-driven and electroosmotic-driven non-Newtonian flows are introduced. In Section 3, the pressure-driven and electroosmotic-driven flows are investigated with the present lattice Boltzmann model and the influences of porosity, solid particle diameters, power law index, yield stress and electric parameters are investigated and discussed. A brief conclusion is given in Section 4.

2. Numerical methods

2.1. The Herschel–Bulkley model for non-Newtonian flow in porous media

For the non-Newtonian fluids exhibiting a yield stress value τ such that a finite pressure gradient, threshold gradient, must be provided before flow can start, we adopt the Herschel–Bulkley model [22]

$$\tau = \eta_0 \dot{\gamma}^n + \tau_0, \quad \tau > \tau_0, \tag{1}$$

where η_0 is the dynamic viscosity, n is the power law exponent, τ_0 is the Bingham fluid yield stress and the local shear rate-related $\dot{\gamma}$ is $\dot{\gamma} = \sqrt{2S_{\alpha\beta}S_{\alpha\beta}}$ with

$$S_{\alpha\beta} = \frac{1}{2}\left(\frac{\partial u_\alpha}{\partial x_\beta} + \frac{\partial u_\beta}{\partial x_\alpha}\right), \tag{2}$$

where $S_{\alpha\beta}$ is the shear strain rate tensor. This model combines power law and Bingham non-Newtonian behavior by adjusting n and τ_0, and can describe most non-Newtonian fluids.

We employ the modified form of Blake–Kozeny equation [22,23] for pressure-driven Herschel–Bulkley fluids of flowing in porous media:

$$\bar{u} = \frac{\varepsilon n}{3n+1}\left(\frac{D_p\varepsilon}{3(1-\varepsilon)}\right)^{1+(1/n)}\left(\frac{\Delta p}{2\eta_0 C' L} - \frac{3(1-\varepsilon)\tau_0}{\varepsilon D_p \eta_0}\right)^{1/n}, \tag{3}$$

where $\bar{u}$ is the average streamwise velocity of the porous media, ε is the porosity, Δp is the pressure difference, D_p is the solid particle diameter, L is the length of the porous media, C' is a constant which accounts for the tortuosity effect of the porous medium and should be determined experimentally and an average $C' = 25/12$ is used [24]. By introducing the definition of permeability

$$K = \frac{\varepsilon^3 D_p^2}{72C'(1-\varepsilon)^2}, \tag{4}$$

and the effective dynamic viscosity

$$\eta_{eff} = \frac{\eta_0}{4}\left(3 + \frac{1}{n}\right)^n (8C'\varepsilon K)^{(1-n)/2}, \tag{5}$$

the model of Eq. (3) simplifies to:

$$\Delta p = \frac{\eta_{eff} L}{K}\bar{u}^n + \sqrt{\frac{\varepsilon C'}{2K}}\tau_0 L. \tag{6}$$

Recall that the Forchheimer flow resistance can be described as the following equation based on the Ergun equation for Newtonian flow in porous media [25],

$$\mathbf{F}_N = -\frac{\upsilon}{K}\mathbf{u} - \frac{F_\varepsilon}{\sqrt{K}}|\mathbf{u}|\mathbf{u}, \tag{7}$$

where υ is the fluid kinematic viscosity, $\mathbf{F}_N$ is the Forchheimer flow resistance for Newtonian fluid, and F_ε is the geometric function of porous media [25]. Similar to this Forchheimer force equation, the flow resistance for Herschel–Bulkley fluids flowing in porous media is stated as

$$\mathbf{F}_{HB} = \frac{\nabla p}{\rho} = -\frac{\eta_{eff}}{\rho K}|\mathbf{u}|^{n-1}\mathbf{u} - \frac{\mathbf{u}}{|\mathbf{u}|}\sqrt{\frac{\varepsilon C'}{2K}}\frac{\tau_0}{\rho}, \tag{8}$$

where ρ is the fluid density and p is the pressure. Nithiarasu et al. [26] adopted a model which is applicable for a medium with both a constant and a variable porosity under the consideration of porosity effect. The model can be expressed by the following equations:

$$\nabla \cdot \mathbf{u} = 0, \tag{9}$$

$$\frac{\partial \mathbf{u}}{\partial t} + (\mathbf{u}\cdot\nabla)\left(\frac{\mathbf{u}}{\varepsilon}\right) = -\frac{1}{\rho}\nabla(\varepsilon p) + \upsilon\nabla^2\mathbf{u} + \varepsilon\mathbf{F}, \tag{10}$$

where $\mathbf{F}$ represents the total body force due to the presence of a porous media and other force fields, and it can be represented using the Herschel–Bulkley force in Eq. (8) if only considering the pressure force.

2.2. The lattice Boltzmann model for porous flow

For the lattice Boltzmann simulation based on the REV scale, Guo and Zhao [11] defined an equilibrium distribution function to include the effect of the porous media,

$$f_i^{eq} = \omega_i\rho\left[1 + \frac{\mathbf{c}_i\cdot\mathbf{u}}{c_s^2} + \frac{(\mathbf{c}_i\cdot\mathbf{u})^2}{2\varepsilon c_s^4} - \frac{|\mathbf{u}|^2}{2\varepsilon c_s^2}\right], \tag{11}$$

where $\omega_0 = 4/9$, $\omega_i = 1/9$ for $i = 1, 2, 3, 4$ and $\omega_i = 1/36$ for $i = 5, 6, 7, 8$. For a D2Q9 square lattice [27], $c_s^2 = c^2/3$ and $\mathbf{c}_0 = 0$, $\mathbf{c}_i = (\cos[(i-1)\pi/2], \sin[(i-1)\pi/2])c$ for $i = 1, 2, 3, 4$ and $\mathbf{c}_i = (\cos[(i-5)\pi/2 + \pi/4], \sin[(i-5)\pi/2 + \pi/4])\sqrt{2}c$ for $i = 5, 6, 7, 8$ where $c = \delta_x/\delta_t$ is the particle streaming speed (δ_x and δ_t are the lattice spacing and time step, respectively).

Adding a force term into the lattice Boltzmann equation to account for the force due to the presence of a porous media, the discretized equation can be written as [11]

$$f_i(\mathbf{x} + \mathbf{c}_i\delta_t, t + \delta_t) - f_i(\mathbf{x}, t) = \frac{1}{\tau_v}[f_i^{eq}(x,t) - f_i(x,t)] + \delta_t F_i, \tag{12}$$

where $\mathbf{x}$ is the position vector, time t, and relaxation time τ_v. The force term F_i is defined in [11,28] for porous flow as

$$F_i = \omega_i\rho\left(1 - \frac{1}{2\tau_v}\right)\left[\frac{\mathbf{c}_i\cdot\mathbf{F}'}{c_s^2} + \frac{\mathbf{u}\mathbf{F}' : (\mathbf{c}_i\mathbf{c}_i - c_s^2\mathbf{I})}{\varepsilon c_s^4}\right]. \tag{13}$$

The density ρ, and velocity $\mathbf{u}$ are obtained from [11]

$$\rho = \sum_i f_i \quad \text{and} \quad \rho\mathbf{u} = \sum_i \mathbf{c}_i f_i + \frac{\delta_t}{2}\rho\mathbf{F}'. \tag{14}$$

We can demonstrate that Eq. (12) recovers the Navier–Stokes Eq. (10) by using the Chapman–Enskog approximation. In this work, we extend this lattice Boltzmann model to non-Newtonian flow. The corresponding relaxation time is

$$\tau_v = 3\frac{\eta_{eff}}{\rho}\frac{\delta_t}{\delta_x^2} + 0.5, \tag{15}$$

If only considering the pressure gradient driving the Herschel–Bulkley fluids in porous media, the external force is stated as

$$\mathbf{F}' = -\frac{\nabla(\varepsilon p)}{\rho} + \varepsilon\mathbf{F}_{HB}. \tag{16}$$

2.3. The porous model for electric potential

Because of no moving component, electroosmosis is often a preferred pumping method for microdevices over pressure-driven flow. Bulk movement of liquid in a microchannel can be achieved by applying an external electric field along the channel. In order to simulate electroosmotic flow driven by the external electricity in porous media at the REV scale, due to the charge of the solid porous material in the channel, it is desirable to remove the charge density's dependence on position at the pore level. An effective charge density ρ_{eff} was obtained which results in the same volume flow in a single pore that would result if the actual charge density had been used [29]

$$\rho_{eff} = \frac{\varepsilon\varepsilon_0\varepsilon_e\zeta_p}{K}\left(\frac{\iint \zeta(r)dA_p}{\zeta_p A_p} - 1\right), \tag{17}$$

where ε_0 is the permittivity of free space, ε_e is the relative dielectric constant of the solution, ζ_p is the zeta potential of the pores, A_p is the cross-sectional area of a single pore, and the integration term takes into consideration double layer effects. The Poisson–Boltzmann equation for the solid porous material can be linearized by assuming that the zeta potential is small enough, then the integration in Eq. (17) is solved analytically and the effective charge density of the solid porous material is expressed as

$$\rho_{eff} = \frac{\varepsilon\varepsilon_0\varepsilon_e\zeta_p}{K}\left(\frac{2I_1(\kappa R_p)}{\kappa R_p I_0(\kappa R_p)} - 1\right), \tag{18}$$

where κ is the reciprocal of the Debye length, I_n is a modified Bessel function of the first type of order n, and R_p is the average pore size calculated by,

$$R_p = \frac{D_p\varepsilon}{3(1-\varepsilon)}. \tag{19}$$

The charge of the solid porous material may change the electric potential distribution between the parallel channels, a modified wall zeta potential, ζ'_w, instead of the zeta potential at the walls of the channel, ζ_w is used

$$\zeta'_w = \zeta_p\left(1 - \frac{2I_1(\kappa R_p)}{\kappa R_p I_0(\kappa R_p)}\right) + \zeta_w - \zeta_p. \tag{20}$$

The relationship between the electric potential in the liquid, ψ, and the modified net charge density per unit volume, ρ_e, at any point in the liquid is described by the Poisson equation:

$$\nabla^2\psi = -\frac{\rho_e}{\varepsilon_0\varepsilon_e}. \tag{21}$$

Assuming that the equilibrium Boltzmann distribution is applicable, the modified net charge density distribution can be expressed as the sum of all the ions in the solution:

$$\rho_e = \sum_\alpha z_\alpha e n_{\alpha,0}\ \exp\left(-\frac{z_\alpha e\psi}{k_B T}\right), \tag{22}$$

where z_α and $n_{\alpha,0}$ are the valence of type α ions and the bulk ionic concentration, respectively. The bulk ionic concentration, n_0 can be expressed as the product of the ionic molar concentration, c_0, and Avogadro's number, N_A. The constant, e, is the charge of a proton, k_B is Boltzmann's constant and T is the absolute temperature. Substituting Eq. (22) into Eq. (21) yields the nonlinear Poisson–Boltzmann equation:

$$\nabla^2\psi + \frac{1}{\varepsilon_0\varepsilon_e}\sum_\alpha z_\alpha e n_{\alpha,0}\ \exp\left(-\frac{z_\alpha e\psi}{k_B T}\right) = 0. \tag{23}$$

This Poisson–Boltzmann equation can be solved similarly with the lattice Boltzmann method (see details in our previous work [30]) and then we can obtain the modified electric potential distribution and the modified charge density per unit volume. In the end, for the electroosmotic-driven Herschel–Bulkley fluid flow in the porous media, by considering both the charge of the solid porous material calculated by Eq. (18) and the modified net charge density of the channel calculated by Eq. (22), in Eqs. (13) and (14) we have

$$\mathbf{F}' = \varepsilon\frac{\mathbf{E}}{\rho}(\rho_{eff} + \rho_e) + \varepsilon\mathbf{F}_{HB}, \tag{24}$$

where $\mathbf{E}$ is the external electricity intensity.

3. Results and discussion

3.1. Pressure-driven Herschel–Bulkley fluids flowing in porous media

First we study the pressure-driven Herschel–Bulkley fluids flowing in porous media, which have numerous significant applications [31]. We set a porous flow between two parallel channels. The channel height $H = 10^{-5}$ m, particle diameter $D_p = 0.1H$, pressure gradient $dp/dx = 10^7$ Pa/m, the porosity $\varepsilon = 0.1$, 0.3, 0.5 and 0.8. We choose the crude oil at 14 degree as the working fluid [23]: $\rho = 891.8$ kg/m^3, $\eta_0 = 0.04054$ kg/m s^{n-2}, $\tau_0 = 0.356$ kg/m s^2, $n = 0.81$. For comparison, we also compute the case of $n = 1.25$ with the other parameters remaining unchanged. The velocity results are shown in Fig. 1, in which the dashed lines represent the solutions of modified Blake–Kozeny Eq. (3) and the solid lines for the LBM results.

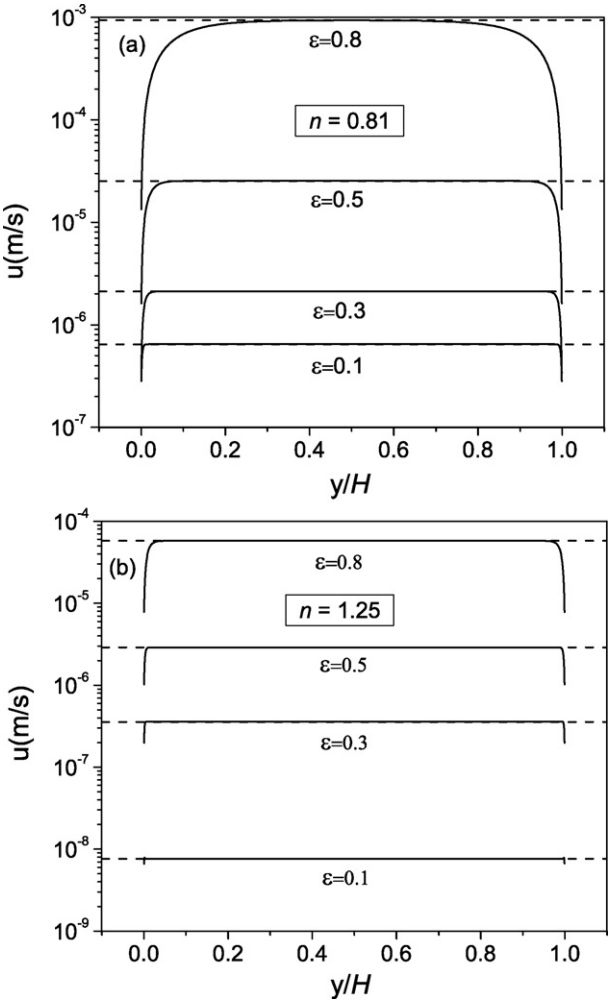

Fig. 1. Comparisons of velocity profiles across the porous channel between the present LBM and Eq. (3). Solid lines are LBM results and dashed lines are solutions of Eq. (3). (a) $n = 0.81$; (b) $n = 1.25$.

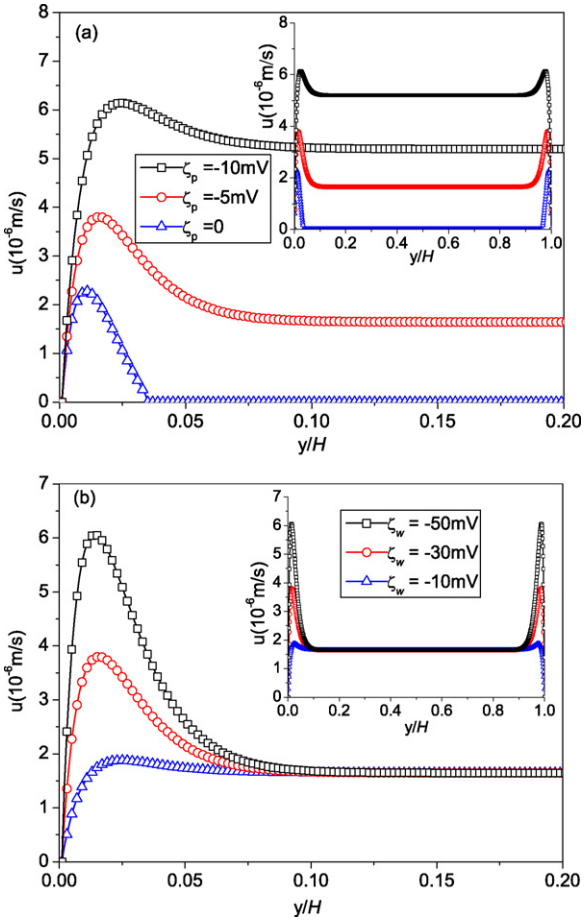

Fig. 2. The velocity distribution at various porous material electric potentials and wall zeta potentials. (a) $\zeta_w = -30$ mV; (b) $\zeta_p = -5$ mV.

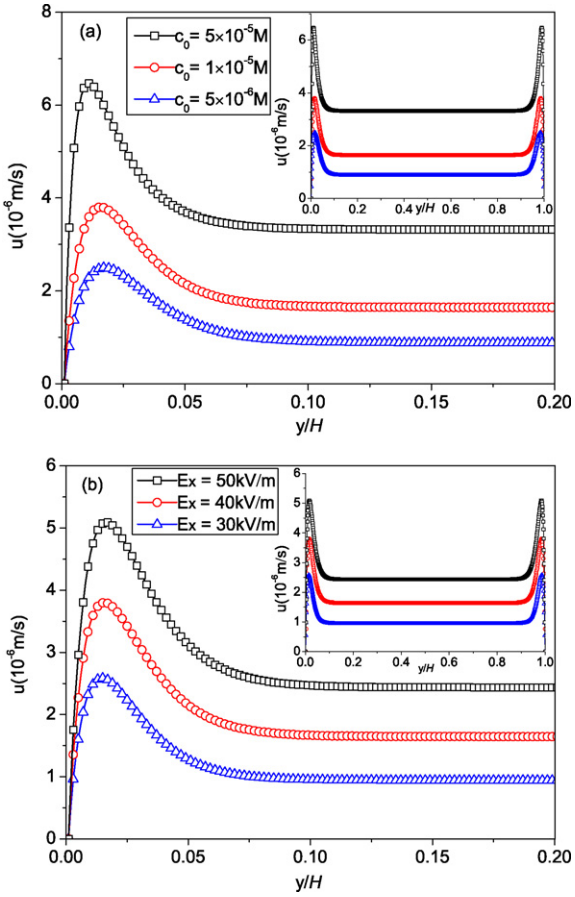

Fig. 3. The velocity distribution at various bulk ionic concentrations and external electric intensities. (a) $E_x = 40$ kV/m; (b) $c_0 = 10^{-5}$ M.

From the figures we can see that as the porosity increases, the porous velocity increases. The LBM results are in good agreement with the solutions from modified Blake–Kozeny Eq. (3) for Herschel–Bulkley fluids, though the LBM can exhibit more details of velocity change close to the wall.

3.2. Electroosmotic flow of Herschel–Bulkley fluids flowing in porous media

In this section, we investigate the porous Herschel–Bulkley fluid flow driven by the external electricity. We choose $T = 293$ K, $z = 1$, $e = 1.6 \times 10^{-19}$ C, $\varepsilon\varepsilon_0 = 7.79 \times 10^{-10}$ C^2/J m, $N_A = 6.02 \times 10^{23}$ mol^{-1}, $k_B = 1.38 \times 10^{-23}$ J/K, $\rho = 997.94$ kg/m^3, $\eta_0 = 983.75 \times 10^{-6}(\sqrt{0.5}s)^{n-1}$ kg/m s. The plane channel height is $H = 10^{-5}$ m, solid particle diameter $D_p = 0.1H$, porosity $\varepsilon = 0.5$, yield stress $\tau_0 = 0.25$ kg/m s^2, power law exponent $n = 0.75$, the bulk ionic concentration $c_0 = 10^{-5}$ M, the external electric intensity parallel to the channel $E_x = 40$ kV/m. In Fig. 2(a) we fix the upper and bottom wall zeta potential $\zeta_w = -30$ mV and change porous material electric potential $\zeta_p = 0$, -5, and -10 mV. In Fig. 2(b) we fix $\zeta_p = -5$ mV and change $\zeta_w = -10$, -30, and -50 mV.

The figures present both the full velocity profiles across the channel and the enlarged section close to the wall for clear view. From Fig. 2(a) we can see that the velocity increases as the porous material electric potential ζ_p increases due to the increase in effective charge density ρ_{eff} as shown in Eq. (18). The velocity close to the wall is much larger than the one in the channel center region since the wall zeta potential ζ_w is larger than the porous material electric potential ζ_p and the total charge density close to the channel wall is larger than that in the center region. We can also see that the bulk fluid remains resting at $\zeta_p = 0$. This is because that the electroosmotic driving force in the center region is very small due to both the zero effective charge density ρ_{eff} at $\zeta_p = 0$ and the quite small modified charge density ρ_e in the channel center region. This small driving force is not able to overcome the non-Newtonian yield stress, or the threshold force.

As seen in Fig. 2(b), we can see that the velocity close to the wall increases as wall zeta potential ζ_w increases due to the increase in modified charge density ρ_e at larger ζ_w. However, the velocity in the channel center region almost remains the same at the shown range of zeta potentials because the zeta wall effect is restricted close to the wall and its effect in the bulk region can be nearly neglected.

In Fig. 3, we study the effect of bulk ionic concentration and the external electric intensity on the velocity. The plane channel height is $H = 10^{-5}$ m, solid particle diameter $D_p = 0.1H$, porosity $\varepsilon = 0.5$, yield stress $\tau_0 = 0.25$ kg/m s^2, power law exponent $n = 0.75$, the upper and bottom channel zeta potential $\zeta_w = -30$ mV, porous material electric potential $\zeta_p = -5$ mV. In Fig. 3(a) we fix $E_x = 40$ kV/m and change the bulk ionic concentration $c_0 = 5 \times 10^{-6}$, 10^{-5}, and 5×10^{-5} M. In Fig. 3(b) we fix $c_0 = 10^{-5}$ M and change $E_x = 30$, 40, and 50 kV/m. From Fig. 3(a) we can see that larger bulk ionic concentration results in larger velocity since both the effective charge density ρ_{eff} and modified charge density ρ_e increase as the bulk ionic concentration increases. In Fig. 3(b), we can see that the velocity increases nearly proportionally as the external electric intensity increases, which means that we can control the flow rate by adjusting the magnitude of the external electric intensity conveniently.

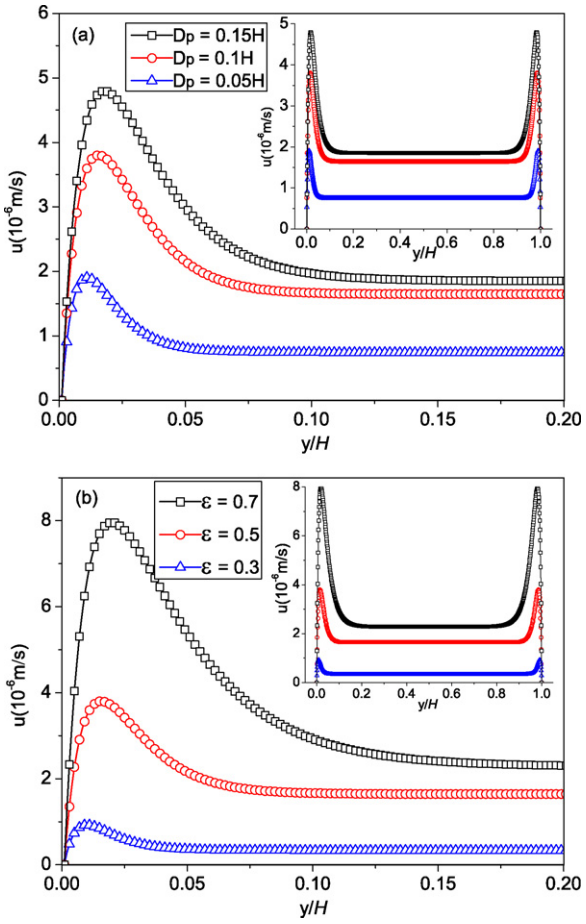

Fig. 4. The velocity distribution at various solid particle diameters and porosities. (a) $\varepsilon = 0.5$; (b) $D_p = 0.1H$.

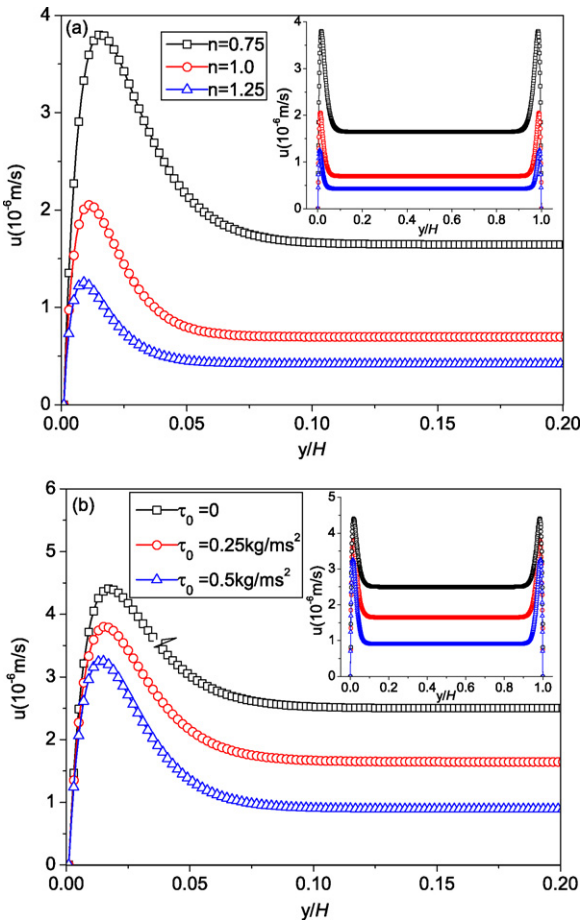

Fig. 5. The velocity distribution at various power law exponents and yield stresses. (a) $\tau_0 = 0.25\ \mathrm{kg/m\,s^2}$; (b) $n = 0.75$.

Fig. 4 presents the effect of solid particle diameter D_p and porosity ε on the porous velocity. We set $H = 10^{-5}$ m, $\tau_0 = 0.25\ \mathrm{kg/m\,s^2}$, power law exponent $n = 0.75$, $\zeta_w = -30$ mV, $\zeta_p = -5$ mV, $c_0 = 10^{-5}$ M, and $E_x = 40$ kV/m. In Fig. 4(a) we fix $\varepsilon = 0.5$ and change $D_p = 0.05H$, $0.1H$, and $0.15H$ while in Fig. 4(b) we fix $D_p = 0.1H$ and change $\varepsilon = 0.3$, 0.5, and 0.8. We can see that the porous velocity increases as the solid particle diameter increases in Fig. 4(a) and as the porosity increases in Fig. 4(b).

It is known that the velocity of pressure-driven flow in porous media is in proportion to the pressure gradient and permeability, and in inverse proportion to the viscosity. Similarly, to investigate the velocity of electroosmotic flow of Herschel–Bulkley fluids in porous media, a reference velocity u_{ref} can be induced, which is in proportion to the electroosmotic force and permeability, and in inverse proportion to the effect dynamic viscosity. The reference velocity u_{ref} can be defined as

$$u_{ref} = \frac{K}{\eta_{eff}} E_x(\rho_e + \rho_{eff}). \tag{25}$$

Using the expression of the effective charge density ρ_{eff} in Eq. (18), the reference velocity u_{ref} can be expressed as

$$u_{ref} = \frac{KE_x\rho_e}{\eta_{eff}} + \frac{E_x\varepsilon\varepsilon_0\varepsilon_e\zeta_p}{\eta_{eff}}\left(\frac{\iint \zeta(r)dA_p}{\zeta_p A_p} - 1\right). \tag{26}$$

As ρ_e is very large near the wall and decreases to zero in the center zone of channel while ρ_{eff} is small near the wall compared with ρ_e and keeps unchanged in the channel, the first term in the right hand side of Eq. (26), marked as u_w, can represent the velocity near the wall, and the second term, marked as u_c, can represent the velocity in the middle of channel.

In Fig. 4(a), the permeability K increases as the solid particle diameter D_p increases at the same porosity, thus u_w increases. The average pore size R_p increases as the solid particle diameter D_p increases, and the term $\left[\iint \zeta(r)dA_p\right]/(\zeta_p A_p)$ in u_c decreases as R_p increases. Because $0 < \left[\iint \zeta(r)dA_p\right]/(\zeta_p A_p) < 1$ and ζ_p is negative, it can be deduced that u_c increases as the solid particle diameter D_p increases.

In Fig. 4(b), the permeability K increases as the porosity ε increases at the same solid particle diameter, so both u_w and u_c increase as the porosity ε increases.

Fig. 5 presents the effect of power law exponent n and yield stress τ_0 on the porous velocity. We set $H = 10^{-5}$ m, $D_p = 0.1H$, $\varepsilon = 0.5$, $\zeta_w = -30$ mV, $\zeta_p = -5$ mV, $c_0 = 10^{-5}$ M, and $E_x = 40$ kV/m. In Fig. 5(a) we fix $\tau_0 = 0.25\ \mathrm{kg/m\,s^2}$ and change $n = 0.75$, 1.0, and 1.25 while in Fig. 5(b) we fix $n = 0.75$ and change $\tau_0 = 0$, 0.25, and $0.5\ \mathrm{kg/m\,s^2}$. Fig. 5(a) shows that the porous velocity decreases as the power law exponent increases since the effective viscosity gets larger as the power law exponent increases. From Fig. 5(b) we can see that the porous velocity decreases as the yield stress increases since larger yield stress counteracts more driving force.

To study the effect of Debye layer length on the porous velocity, we simulate the cases for two different bulk ionic concentrations, $c_0 = 10^{-5}$ and 10^{-6} M at channel height $H = 10^{-6}$ m. The external electric intensity is fixed at $E_x = 400$ kV/m to overcome the very large threshold force for $c_0 = 10^{-6}$ M. Other parameters are $D_p = 0.1H$, $\varepsilon = 0.5$, $\tau_0 = 0.25\ \mathrm{kg/m\,s^2}$, $\zeta_p = -5$ mV, and lower plate wall zeta potential $\zeta_{w1} = -30$ mV. Two magnitudes of power law expo-

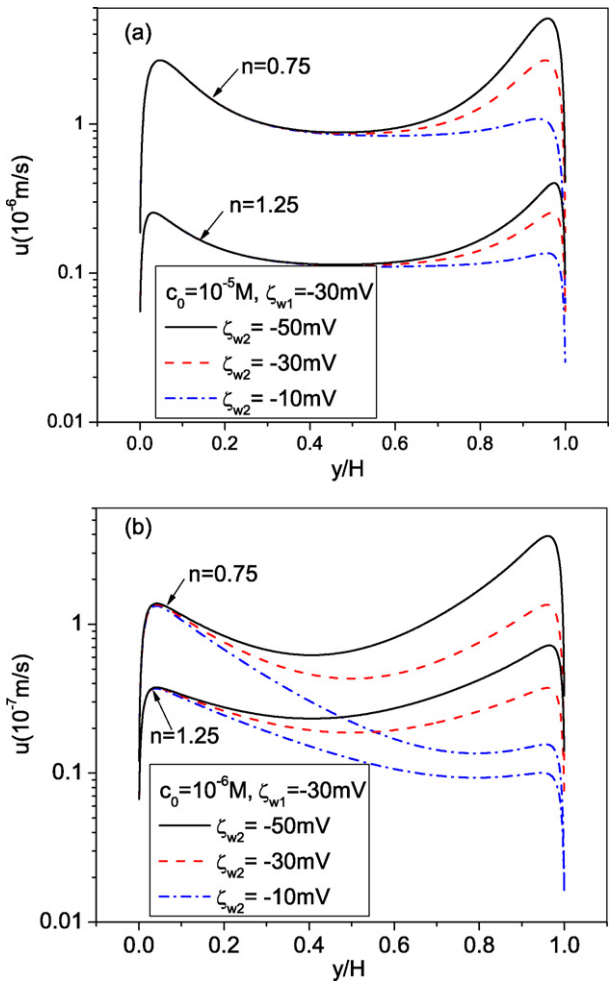

Fig. 6. The velocity distribution at two bulk ionic concentrations for various upper wall zeta potentials. (a) $c_0 = 10^{-5}$ M; (b) $c_0 = 10^{-6}$ M.

nent $n = 0.75$ and 1.25, and three magnitudes of upper plate wall zeta potential $\zeta_{w2} = -10, -30$, and -50 mV are studied. We calculate the Debye layer length with

$$\lambda_D = \sqrt{\frac{\varepsilon_0 \varepsilon_e k_B T}{2N_A c_0 e^2 z^2}}. \quad (27)$$

The corresponding Debye layer length is $\lambda_D = 0.101$ and 0.320 μm for $c_0 = 10^{-5}$ and 10^{-6} M, respectively. The ratio of the channel height to the Debye layer length is 9.9 and 3.125 for $c_0 = 10^{-5}$ and 10^{-6} M, respectively. From Fig. 6(a) we can see that the wall zeta potential effect on the velocity is still restricted within the near wall region since the Debye layer length is very small compared to the channel height. However, as can seen in Fig. 6(b), due to the overlapping effect of the Debye layers originating from the lower plate and upper plate, the zeta wall potential influence goes much deeper into the bulk fluid. From the figures we can also observe that the wall zeta potential effect on the velocity is more sensitive to the lower power law exponent, especially when the ratio of the channel height to the Debye layer length is smaller as shown in Fig. 6(b).

4. Conclusions

In this paper, a lattice Boltzmann algorithm is proposed to simulate pressure-driven and electroosmotic-driven non-Newtonian flow through porous media based on the representative elementary volume scale. The porous media effect was taken into consideration by including the porosity into the equilibrium distribution and adding a non-Newtonian force term to the evolution equation. The non-Newtonian behavior is considered based on the Herschel–Bulkley model, though the present LBM model is straightforward for other non-Newtonian fluid models. For the pressure-driven non-Newtonian porous flow, the LBM results agree well with the analytical solutions, in addition, the LBM results can exhibit more details of the velocity close to the wall.

For the electroosmotic porous flow, the influences of porosity, solid particle diameter, power law exponent, yield stress, zeta wall potential, pore electric potential, external electricity intensity, bulk ionic concentration, and Debye layer length are investigated. The results show that the porous velocity increases as the power law exponent and the yield stress decrease. The electric potential of the porous material has significant effect on the porous velocity in the channel center region while the channel wall zeta potential mainly determines the velocity close the wall. The channel wall zeta potential effect on the velocity is more sensitive to the lower power law exponents, especially at smaller ratio of channel height to the Debye layer length. The results demonstrate that the present lattice Boltzmann model is capable of modeling complicated non-Newtonian flow behaviors through porous media. The further validation by comparing the numerical results with the experimental data is the next work.

Acknowledgments

This work was supported by the National Natural Science Foundation of China (No. 50776067) and by the Program for New Century Excellent Talents in University of China (NCET-07-0676).

References

[1] K. Vafai (Ed.), Handbook of Porous Media, Marcel Dekker, New York, 2000.
[2] D.Q. Li, Electrokinetics in Microfluidics, Elsevier Academic Press, Boston, 2004.
[3] D.H. Rothman, Cellular-automaton fluids—a model for flow in porous-media, Geophysics 53 (1988) 509.
[4] S. Succi, E. Foti, F. Higuera, 3-Dimensional flows in complex geometries with the lattice Boltzmann method, Europhys. Lett. 10 (1989) 433.
[5] S. Succi, Lattice Boltzmann Equation for Fluid Dynamics and Beyond, Clarendon Press, Oxford, 2001.
[6] Q.J. Kang, D.X. Zhang, S.Y. Chen, Unified lattice Boltzmann method for flow in multiscale porous media, Phys. Rev. E 66 (2002) 056307.
[7] J. Bernsdorf, F. Durst, M. Schäfer, Comparison of cellular automata and finite volume techniques for simulation of incompressible flows in complex geometries, Int. J. Numer. Meth. Fluids 29 (1999) 251.
[8] G.H. Tang, W.Q. Tao, Y.L. He, Gas slippage effect on microscale porous flow using the lattice Boltzmann method, Phys. Rev. E 72 (2005) 056301.
[9] G.H. Tang, W.Q. Tao, Y.L. He, Three-dimensional lattice Boltzmann model for gaseous flow in rectangular microducts and microscale porous media, J. Appl. Phys. 97 (2005) 104918.
[10] N. Jeong, Advanced study about the permeability for micro-porous structures using the lattice Boltzmann method, Transp. Porous Media 83 (2010) 271.
[11] Z.L. Guo, T.S. Zhao, Lattice Boltzmann model for incompressible flows through porous media, Phys. Rev. E 66 (2002) 036304.
[12] H.R. Wu, Y.L. He, G.H. Tang, W.Q. Tao, Lattice Boltzmann simulation of flow in porous media on non-uniform grids, Prog. Comput. Fluid Dyn. 5 (2005) 97.
[13] Z.H. Chai, Z.L. Guo, B.C. Shi, Study of electro-osmotic flows in microchannels packed with variable porosity media via lattice Boltzmann method, J. Appl. Phys. 101 (2007) 104913.
[14] D.J. Throckmorton, T.J. Shepodd, A.K. Singh, Electrochromatography in microchips: reversed-phase separation of peptides and amino acids using photopatterned rigid polymer monoliths, Anal. Chem. 74 (2002) 784.
[15] C.H. Chen, J.G. Santiago, A planar electroosmotic micropump, J. Microelectromech. Syst. 11 (2002) 672.
[16] S. Zeng, C.H. Chen, J.C. Mikkelsen Jr., J.G. Santiago, Fabrication and characterization of electroosmotic micropumps, Sens. Actuators B 79 (2001) 107.
[17] L. Chen, J. Ma, F. Tan, Y. Guan, Generating high-pressure sub-microliter flow rate in packed microchannel by electroosmotic force: potential application in microfluidic systems, Sens. Actuators B 88 (2003) 260.
[18] E.S. Boek, J. Chin, P.V. Coveney, Lattice Boltzmann simulation of the flow of non-Newtonian fluids in porous media, Int. J. Mod. Phys. B 17 (2003) 99.
[19] S.P. Sullivan, L.F. Gladden, M.L. Johns, Simulation of power-law fluid flow through porous media using lattice Boltzmann techniques, J. Non-Newtonian Fluid Mech. 133 (2006) 91.

[20] S.P. Sullivan, A.J. Sederman, M.L. Johns, L.F. Gladden, Verification of shear-thinning LB simulations in complex geometries, J. Non-Newtonian Fluid Mech. 143 (2007) 59.
[21] J. Russo, J. Horbach, F. Sciortino, S. Succi, Nanoflows through disordered media: a joint lattice Boltzmann and molecular dynamics investigation, EPL 89 (2010) 44001.
[22] W.H. Herschel, R. Bulkley, Consistency measurements of rubber-benzol solutions, Kolloid-Zeitschrift 39 (1926) 291.
[23] T. Alfariss, K.L. Pinder, Flow through porous-media of a shear-thinning liquid with yield stress, Can. J. Chem. Eng. 65 (1987) 391.
[24] R.E. Hayes, A. Afacan, B. Boulanger, A.V. Shenoy, Modelling the flow of power law fluids in a packed bed using a volume-averaged equation of motion, Transp. Porous Media 23 (1996) 175.
[25] S. Ergun, Fluid flow through packed columns, Chem. Eng. Prog. 48 (1952) 89.
[26] P. Nithiarasu, K.N. Seetharamu, T. Sundararajan, Natural convective heat transfer in a fluid saturated variable porosity medium, Int. J. Heat Mass Transf. 40 (1997) 3955.
[27] Y.H. Qian, D. d'Humieres, P. Lallemand, Lattice BGK models for Navier–Stokes equation, Europhys. Lett. 17 (1992) 479.
[28] Z.L. Guo, C.G. Zheng, B.C. Shi, Discrete lattice effects on the forcing term in the lattice Boltzmann method, Phys. Rev. E 65 (2002) 046308.
[29] N. Scales, R.N. Tait, Modeling electroosmotic and pressure-driven flows in porous microfluidic devices: zeta potential and porosity changes near the channel walls, J. Chem. Phys. 125 (2006) 094714.
[30] G.H. Tang, X.F. Li, Y.L. He, W.Q. Tao, Electroosmotic flow of non-Newtonian fluid in microchannels, J. Non-Newtonian Fluid Mech. 157 (2009) 133.
[31] R.P. Chhabra, J. Comiti, I. Machac, Flow of non-Newtonian fluids in fixed and fluidised beds, Chem. Eng. Sci. 56 (2001) 1.